

Facile preparation of modified Fe-graphene hydrogel with enhanced removal of perfluorooctanoic acid

Xuewen Chen^a, Dan Zhao^{b,*}, Yanmao Dong^b, Yanhui Zhou^b, Yan Yuan^b

^aConstruction Management Institute of Shishan Street and Hengtang Street, Suzhou High-tech Zone, Suzhou, Jiangsu 215011, China, email: 107701178@qq.com

^bSuzhou University of Science and Technology, Suzhou, Jiangsu 215009, China, emails: danny1972820@163.com (D. Zhao), dongyanmao@163.com (Y. Dong), zhouzhouyh222@qq.com (Y. Zhou), 799580172@qq.com (Y. Yuan)

Received 15 May 2021; Accepted 5 September 2021

ABSTRACT

In a facile one-step hydrothermal process, Fe-graphene hydrogel FC1 was prepared through the reaction of graphene and iron ions, besides that, FC2 to FC5 were prepared with the addition of ethylene glycol (EG), EG+NaClO, EG+ ascorbic acid (VC)+NaClO and EG+VC respectively. EG showed to promote the assembly process of graphene hydrogels. The structure of the hydrogel FC4 had the lowest degree of agglomeration and the most porous structure among the samples, indicating that the graphene and iron oxides could support each other with the addition of VC and NaClO. The iron crystals in FC1 and FC5 were α -FeOOH, in FC2 and FC3 were α -FeOOH and Fe_3O_4 , while in FC4 were Fe_3O_4 and Na_3FeO_4 . The perfluorooctanoic acid (PFOA) removal by FC1 to FC5 through Fenton reaction were 73.61%, 75.2%, 84.35%, 89.9% and 75.44% respectively. The PFOA removal through adsorption by FC4 was 41.5%. PFOA removal by FC4 could reach equilibrium in 120 min. Based on the Langmuir model, FC4 had higher maximum adsorption capacity (218.4 mg/g) for PFOA than FC1 (158.3 mg/g). The Fe-graphene hydrogels had excellent removal performance in a wide pH range, and the removal rates were retained well over 5 cycles.

Keywords: Ethylene glycol; Graphene; Hydrogel; Perfluorooctanoic acid

1. Introduction

In recent decades, perfluorooctanoic acid (PFOA) is the representative of perfluorooctanoic acids (PFASs) which is widely used in industry and consumer goods [1–3]. PFASs have high toxicity risks and were classified as persistent organic pollutants (POPs) [4]. Besides its own toxicity risks, Zhuang et al. [5] firstly found that PFASs could lead to structural transformation particles in drinking water and obviously increase the toxicity of particles, which further revealed the necessity to remove PFASs from water. The C–F bond in PFASs had high energy (531.5 kJ/mol), which makes it chemically stable and resistant to traditional treatments [6]. Advanced oxidation processes

(AOPs), which produce strong oxidants at room temperature, have attracted much attention in the degradation of organic pollutants [7]. In AOPs, Fenton reaction had the advantage of simple operation [8]. With the development of nanotechnology, various nanomaterials have been studied as Fenton catalyst. Metal-containing Fenton catalysts (such as those containing copper, cobalt, chromium, cerium and ruthenium) are widely investigated due to their efficient decomposition of H_2O_2 to HO^\bullet . Graphene is an excellent nanomaterial with a large surface area and abundant accessible atoms, and its preparation procedure allows for control over the composition and lateral dimension [9]. In addition to traditional two-dimensional (2D) graphene-based nanomaterials, an increasing number of

* Corresponding author.

three-dimensional (3D) nanostructured graphene-based nanomaterials were demonstrated to exhibit excellent properties for adsorption and catalysis over the years due to their high surface area and easy separation [10]. Establishing graphene-based metal-free Fenton-like catalyst could be helpful to address the problems of the metal-containing Fenton catalysts: (i) the requirement for an acidic solution (pH = 2–4), (ii) the presence of a rate-limiting step causing a low amount of reduction from $M^{(n+m)+}$ to M^{n+} , (iii) the formation of iron-containing sludge and (iv) metal leaching [11]. In addition, two-dimensional graphene-based composite is likely to form a closely stacked structure and is difficult to separate from water after water treatment. Hydrogels, especially inorganic hydrogels, are regarded as outstanding growth matrices for iron oxides because they can establish diffusion-limited conditions to control the morphology and internal structure of the resulting crystals [12]. Graphene oxide (GO) has a two-dimensional (2D) layered structure with sp^2 and sp^3 hybridized carbon atoms arranged in hexagonal rings. Using simple hydrothermal treatments, the 2D GO powders could be turned into 3D reduced GO (RGO) hydrogels through the self-assembly of GO sheets, which restrains the agglomeration of the graphene sheets [13,14]. Moreover, RGO possesses excellent electrical conductivity for fast electron transfer and enhanced visible light response [15].

There are abundant chemical groups on graphene surfaces that make it easy to load other nanomaterials on graphene. Introducing foreign materials into graphene could not only inhibit the aggregation and stacking between individual graphene sheets but also expand the application of these graphene-based nanocomposites in new areas [16]. Among various methods for the preparation of 3D graphene-based nanocomposites, the growth of nanostructures on graphene sheets could overcome the above-mentioned problems due to their mutual support function. EG had been found to effectively enhance Fenton-like property of α -FeOOH/RGO hydrogels and even make it able to generate reactive oxygen species (ROS) without H_2O_2 due to (i) more defects in graphene sheets, (ii) stronger Fe–O–C bonds [17]. Due to the well interaction between iron species and graphene, Fe-graphene based hydrogel has been hot issues among Fenton catalysts [18,19].

Hence, we prepared Fe-graphene hydrogel using EG as assistant under different redox conditions to further modified the structure of the hydrogel. Through various characterizations, we discussed the structure property of the hydrogels. Furthermore, the obtained Fe-graphene hydrogels were used to remove PFOA from water through a heterogeneous Fenton process to evaluate its potential application in water treatment.

2. Materials and methods

All of the chemicals used were analytical grade, and all solutions were prepared using deionized water.

2.1. Preparation of α -FeOOH/RGO hydrogel

GO was prepared from natural powder graphite by a modified Hummers' method. The FC1 hydrogel

was prepared as follows: 20 mg of GO and 0.4 mmol of $FeSO_4 \cdot 7H_2O$ were dispersed into distilled water followed by ultrasonication for approximately 1 h to obtain uniform dispersions. Then, they were transferred into 50 mL Teflon-lined stainless-steel autoclaves and heated in an electric oven at 120°C for 24 h. After the reaction, the autoclaves were cooled down to room temperature. The resulting hydrogels were washed by distilled water. The FC2 hydrogel was prepared as follows: The EG assisted Fe-graphene hydrogel was prepared as follows: 20 mg of GO and 0.4 mmol of $FeSO_4 \cdot 7H_2O$ were dispersed into a 40 mL EG-water mixture (EG to water 1:1) followed by ultrasonication for approximately 1 h to obtain uniform dispersions. Then, they were transferred into 50 mL Teflon-lined stainless-steel autoclaves and heated in an electric oven at 120°C for 24 h. After the reaction, the autoclaves were cooled down to room temperature. The resulting hydrogels were washed by distilled water. The FC3 hydrogel was prepared based on FC2 with the addition of 10 mg NaClO. The FC4 hydrogel was prepared based on FC3 with the addition of 10 mg ascorbic acid (VC). The FC5 hydrogel was prepared based on FC2 with the addition of 10 mg ascorbic acid (VC).

2.2. Materials characterization

The surface morphologies of all the samples were characterized using field-emission scanning electron microscopy (SEM, JEOL, JSM-7001F) and transmission electron microscopy (TEM, jem2100plus). The surface functional groups were observed by Fourier transform infrared spectroscopy (FTIR, Bruker, Vertex 70). The surface elements were analysed using X-ray photoelectron spectroscopy (XPS, ULVAC-PHI, Quantro SXM). The X-ray diffraction (XRD) spectra were collected on a Bragg-Brentano diffractometer (Bruker D8 advance) with monochromatic Cu $K\alpha$ radiation ($\lambda = 0.1542$ nm). The zeta potential of the material was tested by using a zeta potential analyser (Malvern, Zetasizer2000). The specific surface area, pore volume and pore size distribution were tested by nitrogen adsorption/desorption at 77.4 K using an Accelerated Surface Area and Porosimetry system (Micromeritics, ASAP 2020) and were degassed at 373 K for 8 h before the measurements.

2.3. PFOA removal tests

For PFOA degradation, Fe-graphene hydrogels were placed in 10 mg/L PFOA solution containing H_2O_2 (20 mM). The pH values were adjusted to 4–8 (with 6.5 as optimum). After the process, the materials were separated from the solution through a 0.45 μ m membrane. PFOA analysis was performed using an Agilent 1290 Infinity HPLC system coupled to an Agilent 6460 triple quadrupole LC/MS system (Agilent Technologies, Palo Alto, CA) that was operated in negative electrospray ionization (ESI-) mode. The reusability of the Fe-graphene hydrogels were assessed using filtration for regeneration. Typically, after one Fenton cycle, the Fe-graphene hydrogels were filtered out of solution by passage through a 0.22- μ m Millipore filter. The solid material was then washed with deionized water three times, dried at 40°C for 3 h, and reused in the next cycle. Total organic carbon (TOC) was detected by TOC analyzer

(Shimadzu, Japan). The experiments were performed in triplicate. The reported results are the mean of the measured values.

3. Results and discussion

3.1. Morphology characterization

Optical images of the Fe-graphene hydrogels under different initial EG/water ratios are shown in Fig. 1. It can be observed that the all the products are uniform into hydrogels, indicating that the GO could be reduced by FeSO_4 to assemble into hydrogels. At the same time, FeSO_4 could be oxidized by GO into iron oxides [20]. The aqueous solution of FC4 was not clear due to the redox reaction between VC and NaClO. The samples contained EG had larger size than FC1, indicating EG played important role on the formation of the hydrogels. EG could form hydrogen bonds with Fe-graphene hydrogel to induce a more porous and larger structures; furthermore, the hydroxyl groups in EG could help the hydrogel absorb more water. Thus, the addition of EG may help the graphene sheets and iron species to better support each other.

To study the microstructure of the Fe-graphene hydrogels, TEM images of the samples were taken and are shown in Fig. 2. The iron oxides gathered into urchin-like nanorod structures in the samples. In the Fe-graphene hydrogels, the thin plate structure of graphene provides a wide space for iron oxides to be loaded; thus, the spindle-shaped iron oxides are well dispersed in the graphene network. Furthermore, the FC4 shows the lowest degree of agglomeration among the samples, indicating that the graphene and iron oxides could support each other under this condition. To further study the microstructure, SEM results are shown in Fig. 3. It could be seen that FC4 had the most porous structure, which further indicated that the graphene and iron oxides could support each other under this condition. The low agglomeration of the nanorods and porous structure of the hydrogel would help it to have more contact sites.

3.2. Structure analysis

Fig. 4a shows typical XRD patterns of the samples. The reflections of the XRD patterns of FC1 and FC5 are well indexed to the orthorhombic phase of $\alpha\text{-FeOOH}$. The iron crystals in FC2 and FC3 were $\alpha\text{-FeOOH}$ and Fe_3O_4 . The iron oxides in FC4 were Fe_3O_4 and Na_3FeO_4 . FTIR results of the

samples are shown in Fig. 5b. The bands at approximately 640 cm^{-1} correspond to Fe–O stretching vibrations and the bands at approximately 800 and 900 cm^{-1} correspond to the in and out of plane (100) vibrations caused by Fe–OH stretching vibrations, which are characteristic bands of the goethite phase. Peaks at approximately $1,225$ are assigned to the C–O–C vibrations in GO.

XPS analysis was performed to further study the structure of the Fe-graphene hydrogels. The full survey XPS spectra is shown in Fig. 5a. The photoelectron lines at the binding energies of 197.8 , 684.2 , and 712 eV are attributed to the C1s, O1s and Fe2p respectively [21]. As shown in

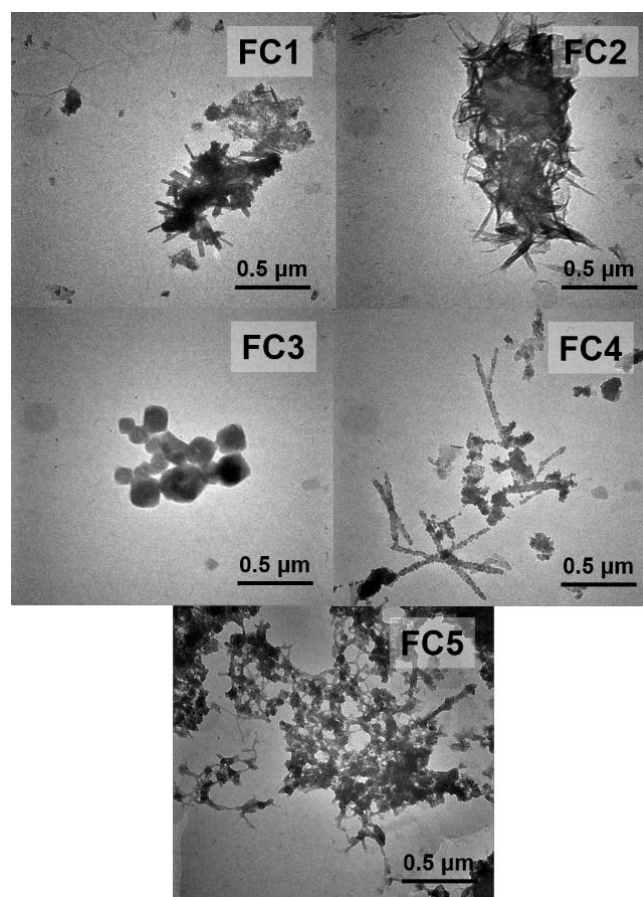


Fig. 2. TEM of the Fe-graphene hydrogels FC1 to FC5.

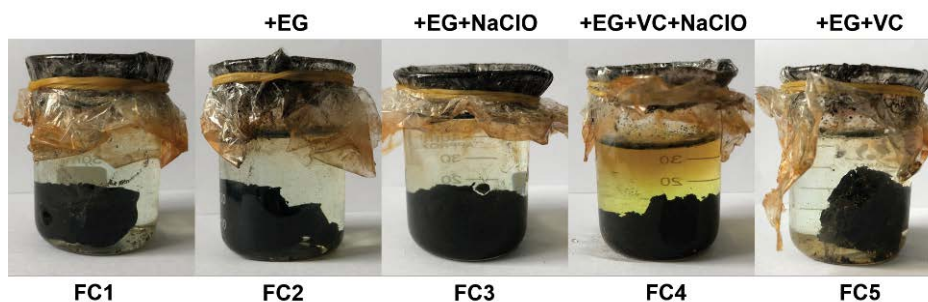


Fig. 1. Optical images of the Fe-graphene hydrogel FC1 to FC5.

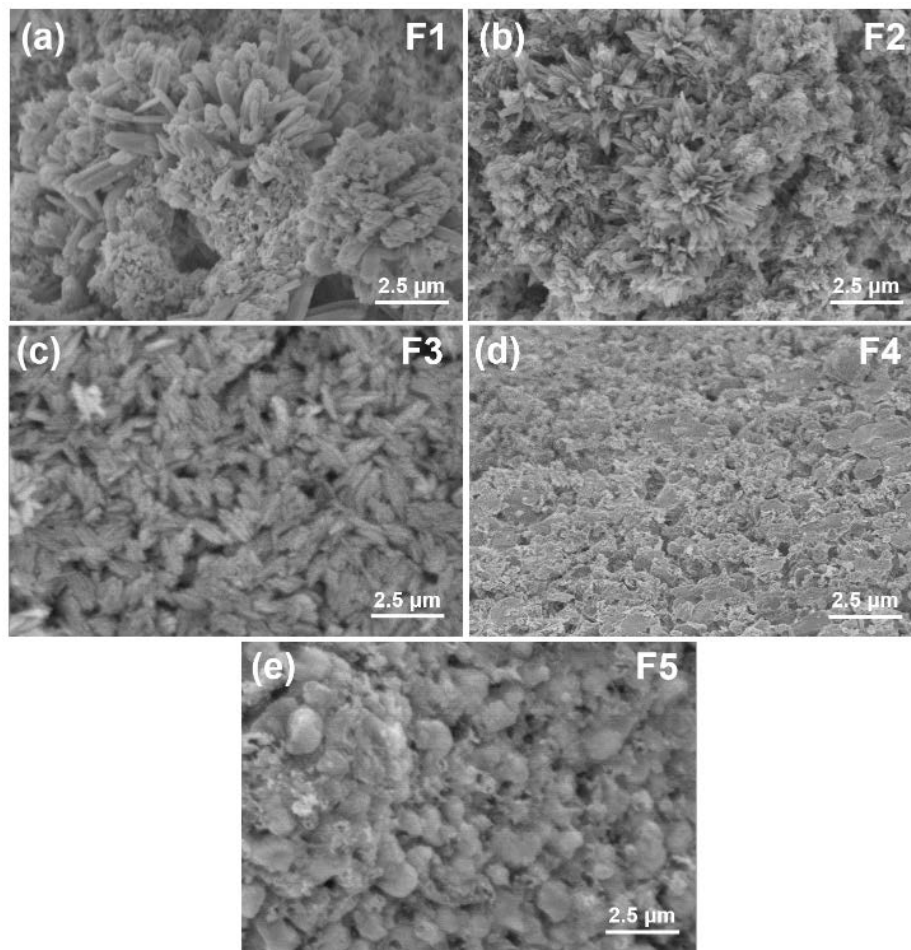


Fig. 3. SEM of the Fe-graphene hydrogels FC1 to FC5.

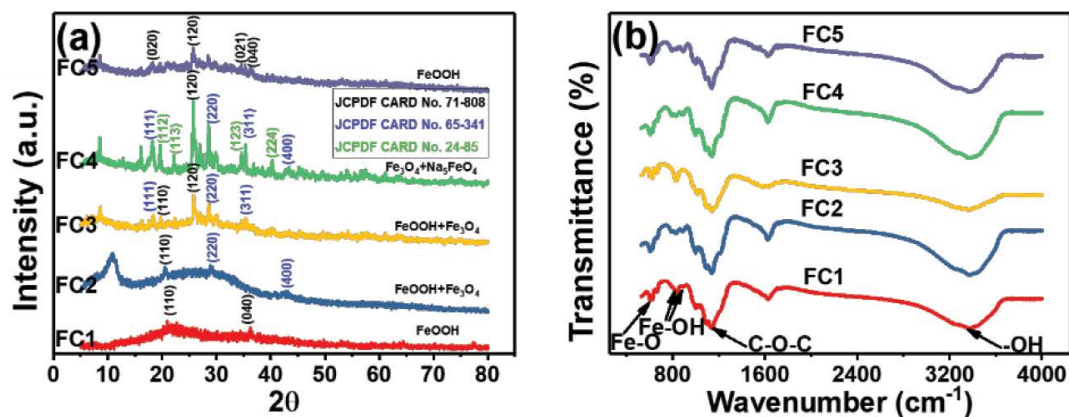


Fig. 4. (a) XRD patterns and (b) FTIR of the Fe-graphene hydrogels FC1 to FC5.

Fig. 6b, the C1s region could be deconvoluted into three overlapped peaks: C=C (sp²) at 284.5 eV, C–O at 286.5 eV and C=O at 287.9 eV [22]. The O1s region could be assigned to Fe–O (530.2 eV), Fe–O–C (531.6 eV), and Fe–OH (532.6 eV), as shown in Fig. 6c, and the presence of Fe–O–C illustrates the linkage between iron species with graphene [23]. In the Fe2p XPS spectrum, as shown in Fig. 5d, the peaks

at 711.1 eV (Fe 2p_{3/2}) and 724.6 eV (Fe 2p_{1/2}) were the characteristic peaks of iron oxides [24].

3.3. PFOA removal through heterogeneous Fenton reaction

The removal rates of PFOA by the Fe-graphene hydrogels are shown in Fig. 6a (PFOA initial concentration

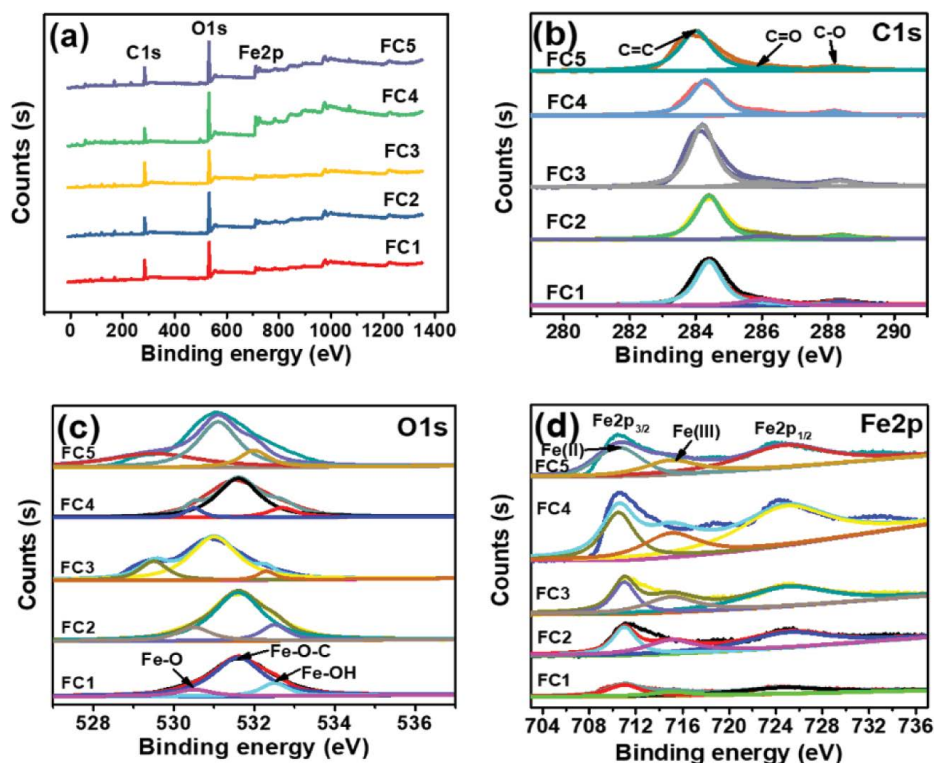


Fig. 5. XPS spectra: (a) full survey XPS spectra, (b) C1s XPS spectra, (c) O1s XPS spectra, and (d) Fe2p XPS spectra.

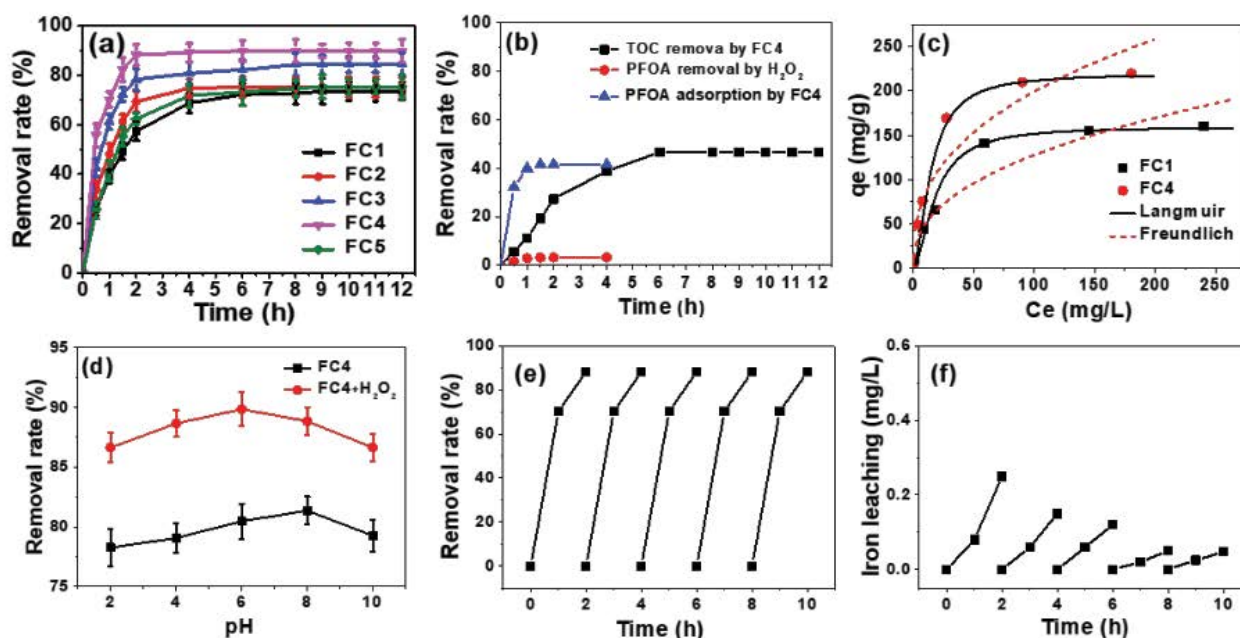


Fig. 6. (a) Removal rates of PFOA by Fe-graphene hydrogels (pH 6, room temperature), (b) PFOA removal by H_2O_2 , PFOA adsorption and chemical oxygen demand removal by FC4 (pH 6, room temperature), (c) Langmuir and Freundlich isotherms, (d) removal rates of PFOA by FC4 at initial different pH values, (e) regeneration property of FC4, and (f) iron leaching during PFOA by FC4.

10 mg/L, H_2O_2 20 mM, pH 6.5). The PFOA removal by FC1 to FC5 through Fenton reaction were 73.61%, 75.2%, 84.35%, 89.9% and 75.44% respectively. Among these Fe-graphene hydrogels, FC4 have the best removal performance. It

can be seen from Fig. 6b that TOC removal by FC4 could reach equilibrium in 120 min. The PFOA removal through adsorption by FC4 was 41.5%. TOC removal by FC4 was 43.57%. The incomplete removal of TOC indicated that

Table 1
Langmuir and Freundlich isotherm parameters of PFOA adsorption on FC1 and FC4

Isotherm model	Parameters	FC1	FC4
Langmuir	q_m (mg/g)	158.3	218.4
	K_L (L/mg)	6.9	9.8
	R^2	0.99	0.96
Freundlich	K_F (L/g)	19.2	9.0
	n	0.5	0.5
	R^2	0.99	0.93

PFOA, although effectively decomposed via this microwave assisted photo-Fenton reaction, may be converted to other organic by-products as reported elsewhere [25]. For example, PFOA degradation may follow a stepwise CF_2 flake-off manner toward short-chain PFOAs under catalytic degradation [26]. Equilibrium adsorption isotherm is one of the most common ways to investigate the adsorption mechanism, to further study the adsorption interaction between the material and PFOA, the adsorption processes are fitted by Langmuir and Freundlich isotherm models as shown in Fig. 6c, and the parameters are shown in Table 1. Through Langmuir model, the R_L value indicates the type of the isotherm to be either favorable ($0 < R_L < 1$), unfavorable ($R_L > 1$), linear ($R_L = 1$), or irreversible ($R_L = 0$) [27]. Values of R_L are found to be less than 1 for FC1 and FC4, which confirms that the PFOA adsorption on Fe-graphene hydrogels were favorable. The applicability of Freundlich isotherm suggests that different sites with several adsorption energies were involved. Based on Langmuir model, FC4 had higher maximum adsorption capacity (218.4 mg/g) for PFOA than FC1 (158.3 mg/g). The maximum adsorption capacity of materials in literature are 16.07 mg/g (magnetic chitosan) [28], 62.5 mg/g (Fe_3O_4 nanoparticles) [29], 1,969 mg/g (Mg-Al hydrotalcites nanosheets) [30]. The main physicochemical properties affecting removal of organic pollutants are pore size (micro and meso) and functional groups [31]. The role of adsorption on Fenton catalysis is to promote the contact between PFOA and the material. The higher adsorption capacity of FC4 could further promote its Fenton degradation of PFOA than FC1. The central Fe ion in material could then react with H_2O_2 to produce a large number of $\cdot OH$ that can attack various chemical bonds in the adsorbed PFOA molecules. The pH value has an important influence on the catalytic performance. The removal rates of PFOA by FC4 at different initial pH values are shown in Fig. 6d, and the removal rate of PFOA by adsorption increases at first and then decreases with increasing pH. The Fe-graphene hydrogels had excellent removal performance in a wide pH range [32–34]. When the initial pH values are below 6, the iron center in the material will react with H^+ and enhance the Fenton catalysis reaction, resulting the increase of removal rate under higher pH. When the initial pH are higher than 8, OH^- ions will be adsorbed by the COOH in PFOA, which could reduce the electrostatic interaction between PFOA and the material and resulting in the decrease of removal

rate [25]. The regeneration property of FC4 is shown in Fig. 6e, which demonstrates that the removal rates were retained well over 5 cycles. Fig. 6f showed the iron leaching during PFOA by FC4. The low concentration of iron leaching reflected that the PFOA degradation was contributed by heterogeneous Fenton reaction.

4. Conclusions

Here, Fe-graphene hydrogels FC1 and FC5 were prepared using a facile one-step hydrothermal process. The iron crystals in FC1 and FC5 were α -FeOOH, in FC2 and FC3 were α -FeOOH and Fe_3O_4 , while in FC4 were Fe_3O_4 and Na_3FeO_4 . The PFOA removal by FC4 was 89.9%, in which adsorption contributed 41.5%. The Fe-graphene hydrogels had excellent removal performance in a wide pH range and had good reuse performance.

Acknowledgements

The author thanks the support of Suzhou Regional Water Quality Improvement and Water Ecological Security Technology and Comprehensive Demonstration Project (2017ZX07205).

Articles in journals

S.W. Lee, S. Sarp, D.J. Jeon and J.H. Kim, Smart water grid: the future water management platform, *Desal. Water Treat.*, 55 (2015) 339–346.

References

- [1] J.P. Giesy, K. Kannan, Global distribution of perfluorooctane sulfonate in wildlife, *Environ. Sci. Technol.*, 35 (2001) 1339–1342.
- [2] K. Kannan, J. Newsted, R.S. Halbrook, J.P. Giesy, Perfluorooctanesulfonate and related fluorinated hydrocarbons in mink and river otters from the United States, *Environ. Sci. Technol.*, 36 (2002) 2566–2571.
- [3] J.W. Martin, D.M. Whittle, D.C.G. Muir, S.A. Mabury, Perfluoroalkyl contaminants in a food web from lake Ontario, *Environ. Sci. Technol.*, 38 (2004) 5379–5385.
- [4] T. Wang, Y.W. Wang, C.Y. Liao, Y.Q. Cai, G.B. Jiang, Perspectives on the inclusion of perfluorooctane sulfonate into the stockholm convention on persistent organic pollutants, *Environ. Sci. Technol.*, 43 (2009) 5171–5175.
- [5] Y. Zhuang, B. Han, R. Chen, B. Shi, Structural transformation and potential toxicity of iron-based deposits in drinking water distribution systems, *Water. Res.*, 165 (2019) 114999, doi: 10.1016/j.watres.2019.114999.
- [6] V.A.A. Espan, M. Mallavarapu, R. Naidu, Treatment technologies for aqueous perfluorooctanesulfonate (PFOS) and perfluorooctanoate (PFOA): a critical review with an emphasis on field testing, *Environ. Technol. Innovation*, 4 (2015) 168–181.
- [7] M. Trojanowicz, A. Bojanowska-Czajka, I. Bartosiewicz, K. Kulisa, Advanced oxidation/reduction Processes treatment for aqueous perfluorooctanoate (PFOA) and perfluorooctanesulfonate (PFOS) – a review of recent advances, *Chem. Eng. J.*, 336 (2018) 170–199.
- [8] G.P. Anipsitakis, D.D. Dionysiou, Radical generation by the interaction of transition metals with common oxidants, *Environ. Sci. Technol.*, 38 (2004) 3705–3712.
- [9] S. Navalon, A. Dhakshinamoorthy, M. Alvaro, M. Antonietti, H. Garcia, Active sites on graphene-based materials as metal-free catalysts, *Chem. Soc. Rev.*, 46 (2017) 4501–4529.
- [10] Y. Zhuang, X. Wang, L. Zhang, Z. Kou, B. Shi, Confinement Fenton-like degradation of perfluorooctanoic acid by a three

- dimensional metal-free catalyst derived from waste, *Appl. Catal., B*, 275 (2020) 119101, doi: 10.1016/j.apcatb.2020.119101.
- [11] L. Lyu, G.F. Yu, L.L. Zhang, C. Hu, Y. Sun, 4-Phenoxyphenol-functionalized reduced graphene oxide nanosheets: a metal-free Fenton-like catalyst for pollutant destruction, *Environ. Sci. Technol.*, 52 (2018) 747–756.
- [12] E. Asenath-Smith, R. Hovden, L.F. Kourkoutis, L.A. Estroff, Hierarchically structured hematite architectures achieved by growth in a silica hydrogel, *J. Am. Chem. Soc.*, 137 (2015) 5184–5192.
- [13] S. Nardecchia, D. Carriazo, M.L. Ferrer, M.C. Gutierrez, F.D. Monte, ChemInform abstract: three dimensional macroporous architectures and aerogels built of carbon nanotubes and/or graphene: synthesis and applications, *Chem. Soc. Rev.*, 42 (2013) 794–830.
- [14] Y. Chen, B. Zhang, G. Liu, X. Zhuang, E.T. Kang, Graphene and its derivatives: switching ON and OFF, *Chem. Soc. Rev.*, 41 (2012) 4688–4707.
- [15] G.K. Pradhan, D.K. Padhi, K.M. Parida, Fabrication of α -Fe₂O₃ Nanorod/RGO composite: a novel hybrid photocatalyst for phenol degradation, *ACS Appl. Mater. Interfaces*, 5 (2013) 9101–9110.
- [16] Y. Ren, C. Zhu, S. Zhang, C. Li, Y. Chen, P. Gao, P. Yang, Q. Ouyang, Three-dimensional SiO₂@Fe₃O₄ core/shell nanorod array/graphene architecture: synthesis and electromagnetic absorption properties, *Nanoscale*, 5 (2013) 12296–12303.
- [17] Y. Zhuang, Q.Z. Liu, Y. Kong, C.C. Shen, H.T. Hao, D.D. Dionysiou, B.Y. Shi, Enhanced antibiotic removal through a dual-reaction-center Fenton-like process in 3D graphene based hydrogels, *Environ. Sci.: Nano*, 6 (2019) 388–398.
- [18] Y. Zhuang, X. Wang, L. Zhang, D.D. Dionysiou, B. Shi, Fe-chelated polymer templated graphene aerogel with enhanced Fenton-like efficiency for water treatment, *Environ. Sci.: Nano*, 6 (2019) 3232–3241.
- [19] Y. Zhuang, X. Wang, L. Zhang, D.D. Dionysiou, Z. Kou, B. Shi, Double-network hydrogel templated FeS/graphene with enhanced PMS activation performance: considering the effect of the template and iron species, *Environ. Sci.: Nano*, 7 (2020) 817–828.
- [20] Y. Zhuang, X. Wang, Q. Liu, B. Shi, N-doped FeOOH/RGO hydrogels with a dual-reaction-center for enhanced catalytic removal of organic pollutants, *Chem. Eng. J.*, 379 (2020) 122310, doi: 10.1016/j.cej.2019.122310.
- [21] F. Liu, S. Chung, G. Oh, T.S. Seo, Three-dimensional graphene oxide nanostructure for fast and efficient water-soluble dye removal, *ACS Appl. Mater. Interfaces*, 4 (2012) 922–927.
- [22] H.P. Cong, X.C. Ren, P. Wang, S.H. Yu, Macroscopic multifunctional graphene-based hydrogels and aerogels by a metal ion induced self-assembly process, *ACS Nano*, 6 (2012) 2693–2703.
- [23] Q. Hui, L. Cao, J. Li, J. Huang, Z. Xu, Y. Cheng, X. Kong, K. Yanagisawa, High pseudo-capacitance in FeOOH/rGO composites with superior performance for high rate anode in li-ion battery, *ACS Appl. Mater. Interfaces*, 8 (2016) 35253–35263.
- [24] G. Huang, C. Zhang, Y. Long, J. Wynn, Y. Liu, W. Wang, J. Gao, Low temperature preparation of α -FeOOH/reduced graphene oxide and its catalytic activity for the photodegradation of an organic dye, *Nanotechnology*, 24 (2013) 395601–395601.
- [25] I.A. Tan, A.L. Ahmad, B.H. Hameed, Adsorption of basic dye on high-surface-area activated carbon prepared from coconut husk: equilibrium, kinetic and thermodynamic studies, *J. Hazard. Mater.*, 154 (2008) 337–346.
- [26] S.C. Smith, D.F. Rodrigues, Carbon-based nanomaterials for removal of chemical and biological contaminants from water: a review of mechanisms and applications, *Carbon*, 91 (2015) 122–143.
- [27] H. Huang, T. Guo, K. Wang, Y. Li, G. Zhang, Efficient activation of persulfate by a magnetic recyclable rape straw biochar catalyst for the degradation of tetracycline hydrochloride in water, *Sci. Total Environ.*, 758 (2021) 143957, doi: 10.1016/j.scitotenv.2020.143957.
- [28] T. Guo, L. Jiang, K. Wang, Y. Li, H. Huang, X. Wu, G. Zhang, Efficient persulfate activation by hematite nanocrystals for degradation of organic pollutants under visible light irradiation: facet-dependent catalytic performance and degradation mechanism, *Appl. Catal., B*, 286 (2021) 119883, doi: 10.1016/j.apcatb.2021.119883.
- [29] T. Guo, L. Jiang, H. Huang, Y. Li, X. Wu, G. Zhang, Enhanced degradation of tetracycline in water over Cu-doped hematite nanoplates by peroxydisulfate activation under visible light irradiation, *J. Hazard. Mater.*, 416 (2021) 125838, doi: 10.1016/j.jhazmat.2021.125838.